Optics Letters

Nonparaxial self-accelerating beams in an atomic vapor with electromagnetically induced transparency

Hua Zhong,[1] Yiqi Zhang,[1,2,*] Zhaoyang Zhang,[1,2] Changbiao Li,[1,2] Da Zhang,[1] Yanpeng Zhang,[1,4] and Milivoj R. Belić[3,5]

[1]Key Laboratory for Physical Electronics and Devices of the Ministry of Education & Shaanxi Key Lab of Information Photonic Technique, Xi'an Jiaotong University, Xi'an 710049, China
[2]Department of Applied Physics, School of Science, Xi'an Jiaotong University, Xi'an 710049, China
[3]Science Program, Texas A&M University at Qatar, P.O. Box 23874 Doha, Qatar
[4]e-mail: ypzhang@mail.xjtu.edu.cn
[5]e-mail: milivoj.belic@qatar.tamu.edu
*Corresponding author: zhangyiqi@mail.xjtu.edu.cn

Received 31 October 2016; revised 10 November 2016; accepted 12 November 2016; posted 14 November 2016 (Doc. ID 279618); published 2 December 2016

We theoretically and numerically investigate the nonparaxial self-accelerating beams in a Λ-type three-level energy system of rubidium atomic vapor in the electromagnetically induced transparency (EIT) window. In the EIT window, the absorption of the atomic vapor is small, and robust nonparaxial self-accelerating beams can be generated. The reason is that the energy of the tail transfers to the main lobe, which then maintains its shape, owing to the self-healing effect. Media with large absorption would demand large energy to compensate, and the tail would be lifted too high to maintain the profile of an accelerating beam, so that self-accelerating beams cannot be obtained any longer. An atomic vapor with small absorption is the ideal medium to produce such self-accelerating beams and, in return, self-accelerating beams may inspire new ideas in the research associated with atomic vapors and atomic-like ensembles.

OCIS codes: (070.3185) Invariant optical fields; (140.3300) Laser beam shaping; (350.5500) Propagation; (300.1030) Absorption.

https://doi.org/10.1364/OL.41.005644

Being convenient optical media for various applications, atomic vapors were intensely investigated in the last few decades [1]. To overcome large absorption in atomic vapors, electromagnetically induced transparency (EIT) [2] was developed. EIT plays an important role in generating multi-wave mixing processes [3,4]. Recently, interesting experiments have been carried out in atomic vapors, including an EIT-enhanced four-wave mixing (FWM) in rubidium vapor [5,6], an efficient six-wave mixing (SWM) in a five-level close-cycled atomic system [4], and coexisting FWM and SWM in two ladder-type EIT windows [7]. In addition, optical vortices [8,9], optical condensates [10,11], photonic topological insulators [12–14], (anti-) parity-time symmetry [15–17], and other interesting phenomena [18,19] have also been observed in atomic vapors. Of these other interesting phenomena, one should mention the generation of self-accelerating and nondiffracting Airy beams [20–23] in atomic vapors [24–31].

Unfortunately, a paraxial Airy beam attenuates quickly when propagating in an atomic vapor, even when absorption is small (i.e., in the EIT window); that is, it is not loss-proof. From this point of view, absorption limits the application of atomic vapors. Nevertheless, there exist loss-proof self-accelerating beams in the lossy media [32] which could propagate robustly, but they are of a different type. Such self-accelerating beams originate from the complex Bessel function or other special functions, represent eigenmodes of the lossy media, and belong to the family of nonparaxial accelerating beams. We believe that such nonparaxial self-accelerating beams may exist in an atomic vapor, which is a natural optical medium (contains no free charges or conduction currents) for the production of the loss-proof self-accelerating beams. This exactly is the goal of investigation in this Letter.

Thus, we demonstrate the existence of nonparaxial self-accelerating beams in atomic vapors with small absorption in the EIT window. As an example, we consider first the case of a beam that accelerates along a circular trajectory. Then we provide a general discussion and numerical simulation of such self-accelerating beams. In the end, we display nonparaxial accelerating beams that accelerate along parabolic and elliptic trajectories. Due to the multi-parameter controllable properties of an atomic vapor, our research may broaden the field of potential applications of self-accelerating beams in atomic vapors. We also believe that such beams can be utilized in on-chip crystals, for example, in the praseodymium-doped yttrium orthosilicate crystal [33,34], which exhibits properties similar to atomic vapors.

The wave equation in an optical medium can be written as [35]

$$\nabla^2\mathbf{E} - \frac{1}{c^2}\frac{\partial^2\mathbf{E}}{\partial t^2} = \frac{1}{\epsilon_0 c^2}\frac{\partial^2\mathbf{P}}{\partial t^2}, \tag{1}$$

where ∇^2 is the Laplacian, ϵ_0 is the permittivity in vacuum, c is the light speed in vacuum, and $\mathbf{P}$ is the polarization vector. When only the linear polarization is considered, one obtains $\mathbf{P} = \epsilon_0\chi^{(1)}\mathbf{E}$, where $\chi^{(1)}$ is the linear susceptibility. We restrict our attention to the two-dimensional case of Eq. (1) and seek the TE-polarized solutions of the form $\mathbf{E}(x, y, z) = E_y(x, z)\mathbf{y}$. Then, Eq. (1) can be rewritten as

$$\left(\frac{\partial^2}{\partial z^2} + \frac{\partial^2}{\partial x^2}\right)E_y - \frac{1}{c^2}\frac{\partial^2 E_y}{\partial t^2} = \frac{\chi^{(1)}}{c^2}\frac{\partial^2 E_y}{\partial t^2}. \tag{2}$$

This being a linear partial differential equation, the optical field E_y can be sought in the harmonic form $E_y = \psi\exp(i\omega t)$, so that Eq. (2) becomes

$$\left(\frac{\partial^2}{\partial z^2} + \frac{\partial^2}{\partial x^2}\right)\psi + k^2[1 + \chi^{(1)}]\psi = 0, \tag{3}$$

where $k = \omega/c$ is the linear dispersion relation. Equation (3) is the well-known two-dimensional Helmholtz equation. Our research can be easily extended to three dimensions.

We consider the propagation in a Λ-type rubidium atomic vapor [13,36,37], as shown in Fig. 1(a). The linear susceptibility in this case can be written as

$$\chi^{(1)} = \frac{iN\mu_{10}^2}{\hbar\epsilon_0}\frac{1}{d_{10} + |G_{12}|^2/d_{20}}, \tag{4}$$

with N being the atomic density, μ_{10} being the electric dipole moment, and $d_{10} = \Gamma_{10} + i\Delta_{10}$ and $d_{20} = \Gamma_{20} + i(\Delta_{10} - \Delta_{12})$ the complex decay rates. In Fig. 1(a), the probe field E_{10} connects the transition $|0\rangle \to |1\rangle$, and the coupling field E_{12} connects the transition $|1\rangle \to |2\rangle$. Γ_{ij} are the decay rates between the $|i\rangle$ and $|j\rangle$ states, and $\Delta_{10} = \Omega_{10} - \omega_{10}$ and $\Delta_{12} = \Omega_{12} - \omega_{12}$ are the detunings. They are determined by the transition frequencies Ω_{ij} between $|i\rangle$ and $|j\rangle$, and by the frequencies ω_{10} and ω_{12} of the probe and the coupling fields. G_{12} represents the Rabi frequency of the coupling fields, defined as $G_{12} = \mu_{12}E_{12}/\hbar$.

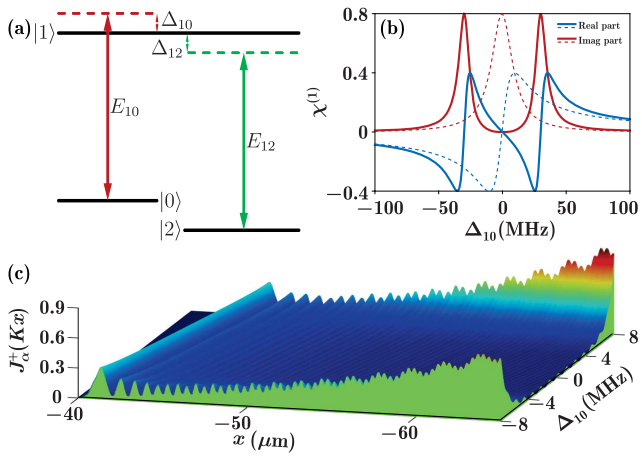

Fig. 1. (a) Λ-type energy system in a rubidium atomic vapor. (b) Linear susceptibility $\chi^{(1)}$. The parameters are $N = 5\times10^{13}\,\mathrm{cm}^{-3}$, $\mu_{12} = 1.22\times10^{-29}$ C·m, $\Gamma_{10} = 1$ MHz, $\Gamma_{20} = 1$ kHz, and $\Delta_{12} = 0$. The solid and dashed curves are for $G_{12} = 30$ MHz and $G_{12} = 0$. (c) Complex half-Bessel function as a function of x and Δ_{10} in the EIT window with $\alpha = 500$.

In Fig. 1(b), we display the linear susceptibility $\chi^{(1)}$. If $G_{12} \neq 0$, there is an EIT window, as shown by the red solid curve and, at the two-photon resonance condition $\Delta_{10} - \Delta_{12} = 0$, the absorption is much decreased, seemingly zero. Still, it should be noted that some residual absorption always remains in the EIT window. As a result, Eq. (3) is the Helmholtz equation in the weakly lossy media. In this Letter, we only consider the case of the EIT window. If $G_{12} = 0$, the absorption in the atomic vapor is quite large, as indicated by the red dashed curve.

Recently, several interesting accelerating solutions of the Helmholtz equation have been developed [38–41]. Without the loss of generality, we first consider an accelerating solution along a circular trajectory; later, we provide a discussion on the parabolic and elliptic trajectories. In polar coordinates, Eq. (3) can be rewritten as

$$\frac{1}{r}\frac{\partial}{\partial r}\left(r\frac{\partial\psi}{\partial r}\right) + \frac{1}{r^2}\frac{\partial^2\psi}{\partial\theta^2} + k^2[1 + \chi^{(1)}]\psi = 0, \tag{5}$$

after performing a coordinate transformation $z = r\sin\theta$ and $x = r\cos\theta$. For the circularly accelerating beams, we seek solutions in the form $\psi = U(r)\exp(i\alpha\theta)$, where α is a free real parameter. In this manner, Eq. (5) is recast into

$$r\frac{\partial}{\partial r}\left(r\frac{\partial U}{\partial r}\right) + (-\alpha^2 + r^2k^2[1 + \chi^{(1)}])U = 0. \tag{6}$$

According to previous literature [32,38,42], an exact solution of Eq. (6) is the complex Bessel function of the order α, i.e., $U(r) = J_\alpha(rK)$ with $K^2 = k^2[1 + \chi^{(1)}]$. To properly introduce initial conditions, we utilize only the half-Bessel propagating solution that has the form [43]

$$J_\alpha^+(Kx, Kz) = \int_{-\pi/2}^{\pi/2}\exp(i\alpha\theta)\exp[iK(x\sin\theta + z\cos\theta)]\mathrm{d}\theta. \tag{7}$$

In Fig. 1(c), we display the half-Bessel function $J_\alpha^+(Kx)$ in the EIT window. One finds that the tail of the solution lifts higher and higher when it approaches the boundary of the EIT window (with an increasing absolute value of Δ_{12}). Numerical simulations demonstrate that the solution loses its Bessel profile as the absorption gets larger. The reason is that the energy moves from the tail to the main lobe during propagation to compensate for the absorption losses, as an indication of the self-healing effect [32]. The larger the absorption, the higher the tail, to supply enough energy to heal the main lobe during propagation. As a result, the tail eventually becomes too high to maintain the Bessel profile when the absorption gets too large. Therefore, we have to consider self-accelerating beams in the EIT window that guarantees small absorption.

We first consider the self-accelerating solution at the two-photon resonance point, with $\Delta_{10} = \Delta_{12} = 0$. One calculates the linear susceptibility $\chi^{(1)} \approx i8.8646\times10^{-6}$, which is indeed small. The corresponding effective wavenumber is $K \approx 1.181\times10^7 + i5.2348\times10^1\ \mathrm{m}^{-1}$. The propagation of the beam, obtained using Eq. (7) at $z = -20$ μm, is shown in Fig. 2(a). One finds that the beam indeed accelerates along a circular trajectory (the white dashed curve), with the beam shape preserved in the wide angle range, up to [−40°, 40°]. (We set the red dashed line as 0°, which is the symmetry axis of the trajectory.) We point out that if a proper truncation is used, which removes more

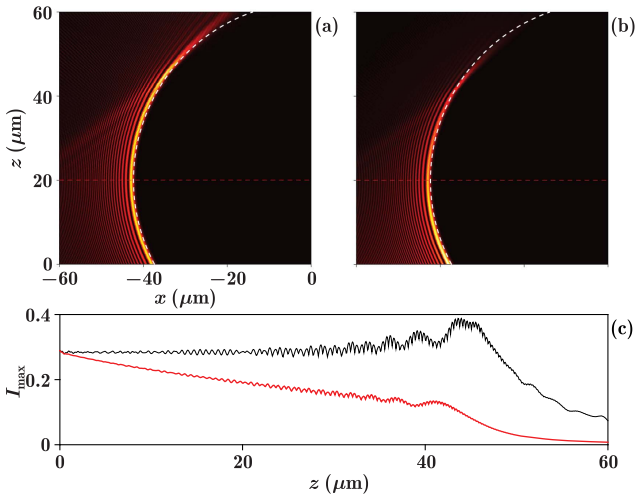

Fig. 2. (a) Propagation of the circular self-accelerating beam in the medium with $\Delta_{10} = \Delta_{12} = 0$. (b) Propagation of the same beam, but in the medium with $\Delta_{10} = 4$ MHz and $\Delta_{12} = 0$. The white dashed curve shows the analytical trajectory, the red dashed line indicates the symmetry axis of the trajectory. (c) Maximum intensity of the beam during propagation. The black curve and the red curve correspond to (a) and (b), respectively.

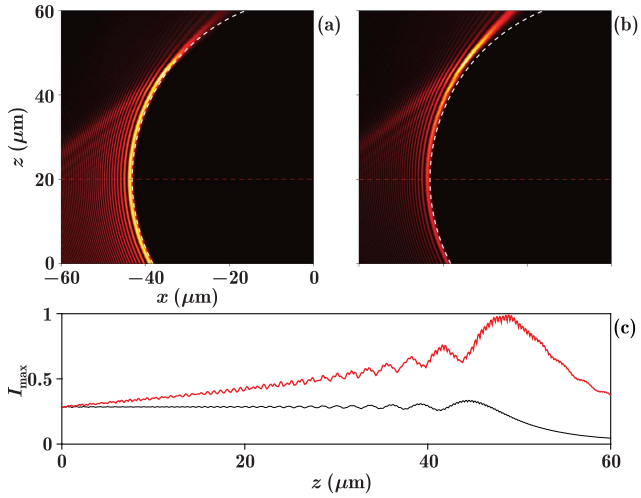

Fig. 3. (a) Propagation of the self-accelerating beam with $\Delta_{10} = 4$ MHz and $\Delta_{12} = 0$. (b) Propagation of the same beam, but in the medium with $\Delta_{10} = \Delta_{12} = 0$. (c) Maximum intensities in (a) and (b).

energy from the tail, the shape-preserving range can be much broadened. For comparison, one may find the solution directly from Eq. (7); however, this solution is not a physical quantity because it carries infinite energy.

Using the same input as in Fig. 2(a), we check its propagation under the condition $\Delta_{10} = 4$ MHz and $\Delta_{12} = 0$, which leads to $\chi^{(1)} = -0.0360 + i0.0016$ and $K = 1.1596 \times 10^7 + i9.8597 \times 10^3\ \mathrm{m}^{-1}$. Clearly, such a condition corresponds to a much bigger absorption than at the two-photon resonance condition. As shown by the numerically simulated propagation in Fig. 2(b), the beam attenuates gradually. In Fig. 2(c), we plot the maximum intensity of the beam recorded during propagation, from which one finds that the maximum intensity in Fig. 2(a) is maintained quite well, while that in Fig. 2(b) decreases appreciably.

Now, different from Fig. 2, we first consider the self-accelerating beam and its propagation under the condition $\Delta_{10} = 4$ MHz and $\Delta_{12} = 0$, and then follow the propagation under the two-photon resonance condition. The results are displayed in Figs. 3(a) and 3(b). Recall that in Fig. 2(a) the beam is the mode of the medium right at the EIT condition, so its intensity changes little. In Fig. 2(b), the input is the same as in Fig. 2(a), but it propagates in a lossy medium, so the intensity decreases. One finds that the propagation in Fig. 3(a) is quite similar to that in Fig. 2(a); the beam accelerates along a circular trajectory with the shape preserved because, in both cases, the input beams are the modes of the system, regardless of the absorption, if the truncation is not considered. In Fig. 3(b), the beam still accelerates along a circular trajectory, but the intensity of the main lobe increases during propagation. The reason is that the absorption of the system in Fig. 3(b) is smaller than that in Fig. 3(a), and the energy transferred from the tail to the main lobe overcompensates the absorption. As explained in [32], the propagation in Figs. 2(a) and 3(a) is the indication of the self-healing effect; those in Figs. 2(b) and 3(b) are indications of the under-healing and over-healing. Maximum intensities recorded during propagation also demonstrate these effects, as exhibited in Figs. 2(c) and 3(c).

Up to now, we have considered the nonparaxial self-accelerating beams in atomic vapors which accelerate along circular trajectories in the EIT window. As it is well known, there also exist nonparxial self-accelerating beams that accelerate along parabolic and elliptic trajectories, the Weber and Mathieu beams [39,40,44]. They arise when the eigensolutions of the Helmholtz Eq. (3) that separate in the parabolic and elliptic coordinate systems are considered. An extension to three dimensions would require the separation of solutions of the three-dimensional Helmholtz equation in cylindrical, parabolic cylindrical, and elliptic cylindrical coordinates [45]. We still restrict our attention to the two-dimensional cases. Therefore, it is of interest to investigate such beams in lossy atomic vapors. In Figs. 4(a1)–4(c1) and 4(a2)–4(c2), the loss-proof self-accelerating beams that accelerate along parabolic and elliptic trajectories are displayed. The concrete settings are elucidated in the caption. As expected, the results indeed show the under-healing and over-healing effects. The two-dimensional loss-proof self-accelerating beam family in atomic vapors, as displayed in this Letter, consists of the self-accelerating beams that accelerate along circular, parabolic, and elliptic trajectories.

In summary, we have investigated the nonparaxial self-accelerating beams in atomic vapors in the EIT window. Even though there is absorption, the nonparaxial accelerating beams may propagate robustly in atomic vapors, due to the fact that such beams are eigenmodes of the Helmholtz equation in the media with absorption. Beyond the EIT window, such nonparaxial accelerating beams do not exist because the compensation of the absorption needs a large energy transfer from the tail to the head of the beam. As a result, the tail has to be lifted too high to maintain the shape of the self-accelerating beam, which cannot be achieved at high absorptions. Our method can be naturally extended to three dimensions. The self-accelerating beams in atomic vapors broaden the application potential of atomic vapors and inspire new ideas in research associated with

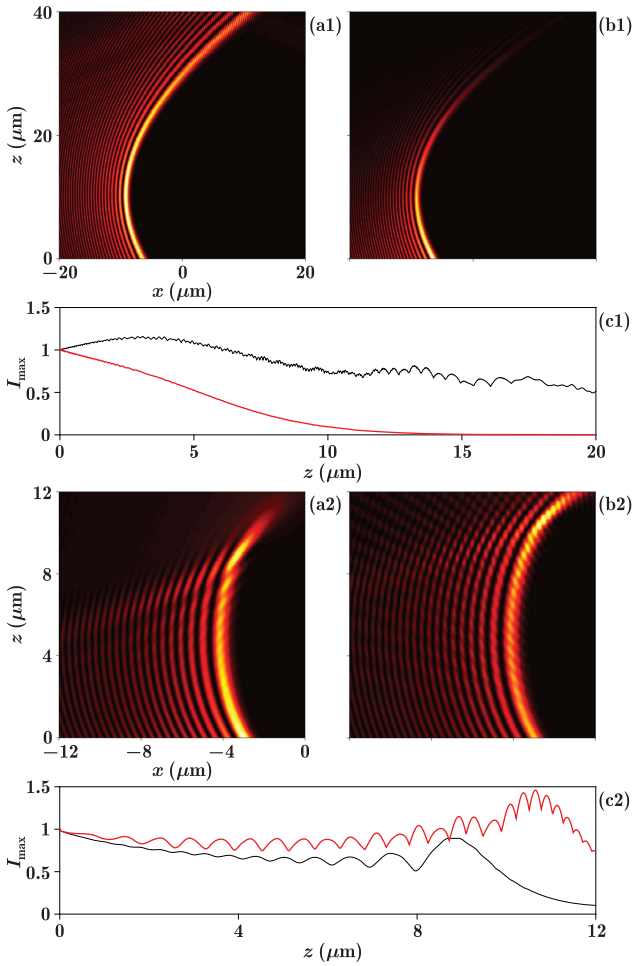

Fig. 4. (a1)–(c1) Setup is as in Fig. 2, but for the self-accelerating Weber beam of order 100. (a2) and (c2) Setup is as in Fig. 3, but for the self-accelerating half-Mathieu beam of the order 65 and with foci (± 6 μm, 0). We use $\Delta_{10} = 6$ MHz in (b1) and (a2).

atomic vapors or other atomic-like solid media (e.g., the praseodymium-doped yttrium orthosilicate crystal).

Funding. National Natural Science Foundation of China (NSFC) (61308015, 61605154, 11474228); Key Scientific and Technological Innovation Team of Shaanxi Province (2014KCT-10); China Postdoctoral Science Foundation (2016M590935); Qatar National Research Fund (QNRF) (NPRP 6-021-1-005).

REFERENCES

1. M. Fleischhauer, A. Imamoglu, and J. P. Marangos, Rev. Mod. Phys. **77**, 633 (2005).
2. S. E. Harris, Phys. Today **50**(7), 36 (1997).
3. M. D. Lukin, A. B. Matsko, M. Fleischhauer, and M. O. Scully, Phys. Rev. Lett. **82**, 1847 (1999).
4. H. Kang, G. Hernandez, and Y. Zhu, Phys. Rev. A **70**, 061804 (2004).
5. P. R. Hemmer, D. P. Katz, J. Donoghue, M. S. Shahriar, P. Kumar, and M. Cronin-Golomb, Opt. Lett. **20**, 982 (1995).
6. M. Jain, H. Xia, G. Y. Yin, A. J. Merriam, and S. E. Harris, Phys. Rev. Lett. **77**, 4326 (1996).
7. Y. P. Zhang, A. W. Brown, and M. Xiao, Phys. Rev. Lett. **99**, 123603 (2007).
8. Y. Q. Zhang, Z. K. Wu, C. Z. Yuan, X. Yao, K. Q. Lu, M. Belić, and Y. P. Zhang, Opt. Lett. **37**, 4507 (2012).
9. Y. Q. Zhang, M. Belić, Z. K. Wu, C. Z. Yuan, R. M. Wang, K. Q. Lu, and Y. P. Zhang, Phys. Rev. A **88**, 013847 (2013).
10. H. Michinel, M. J. Paz-Alonso, and V. M. Pérez-García, Phys. Rev. Lett. **96**, 023903 (2006).
11. Z. K. Wu, Y. Q. Zhang, C. Z. Yuan, F. Wen, H. B. Zheng, Y. P. Zhang, and M. Xiao, Phys. Rev. A **88**, 063828 (2013).
12. G. Jotzu, M. Messer, R. Desbuquois, M. Lebrat, T. Uehlinger, D. Greif, and T. Esslinger, Nature **515**, 237 (2014).
13. Y. Q. Zhang, Z. K. Wu, M. R. Belić, H. B. Zheng, Z. G. Wang, M. Xiao, and Y. P. Zhang, Laser Photon. Rev. **9**, 331 (2015).
14. D.-W. Wang, H. Cai, L. Yuan, S.-Y. Zhu, and R.-B. Liu, Optica **2**, 712 (2015).
15. C. Hang, G. Huang, and V. V. Konotop, Phys. Rev. Lett. **110**, 083604 (2013).
16. Z. Y. Zhang, Y. Q. Zhang, J. T. Sheng, L. Yang, M.-A. Miri, D. N. Christodoulides, B. He, Y. P. Zhang, and M. Xiao, Phys. Rev. Lett. **117**, 123601 (2016).
17. P. Peng, W. Cao, C. Shen, W. Qu, J. Wen, L. Jiang, and Y. Xiao, Nat. Phys. (2016).
18. D.-W. Wang, H.-T. Zhou, M.-J. Guo, J.-X. Zhang, J. Evers, and S.-Y. Zhu, Phys. Rev. Lett. **110**, 093901 (2013).
19. J.-H. Wu, M. Artoni, and G. C. La Rocca, Phys. Rev. Lett. **113**, 123004 (2014).
20. G. A. Siviloglou and D. N. Christodoulides, Opt. Lett. **32**, 979 (2007).
21. G. A. Siviloglou, J. Broky, A. Dogariu, and D. N. Christodoulides, Opt. Lett. **33**, 207 (2008).
22. Y. Q. Zhang, M. R. Belić, J. Sun, H. B. Zheng, Z. K. Wu, H. X. Chen, and Y. P. Zhang, Rom. Rep. Phys. **67**, 1099 (2015).
23. F. Diebel, B. M. Bokić, D. V. Timotijević, D. M. J. Savić, and C. Denz, Opt. Express **23**, 24351 (2015).
24. F. Zhuang, J. Shen, X. Du, and D. Zhao, Opt. Lett. **37**, 3054 (2012).
25. Y.-Y. Li, L. Li, Y.-X. Lu, X.-X. Zhao, K.-W. Xu, Y.-Q. Zhang, and Y.-P. Zhang, Opt. Express **21**, 8311 (2013).
26. C. Hang and G. Huang, Phys. Rev. A **88**, 013825 (2013).
27. C. Hang and G. Huang, Phys. Rev. A **89**, 013821 (2014).
28. C. Hang, Z. Bai, and G. Huang, Phys. Rev. A **90**, 023822 (2014).
29. D. Wei, Y. Yu, M. Cao, L. Zhang, F. Ye, W. Guo, S. Zhang, H. Gao, and F. Li, Opt. Lett. **39**, 4557 (2014).
30. L. Zhang, F. Ye, M. Cao, D. Wei, P. Zhang, H. Gao, and F. Li, Opt. Lett. **40**, 5066 (2015).
31. D. Wei, J. Liu, Y. Yu, J. Wang, H. Gao, and F. Li, J. Phys. B **48**, 245401 (2015).
32. R. Schley, I. Kaminer, E. Greenfield, R. Bekenstein, Y. Lumer, and M. Segev, Nat. Commun. **5**, 5189 (2014).
33. H. Y. Lan, C. B. Li, C. J. Lei, H. B. Zheng, R. M. Wang, M. Xiao, and Y. P. Zhang, Laser Phys. Lett. **12**, 015404 (2015).
34. C. B. Li, L. L. Wang, C. Yang, T. Jiang, M. Imran, I. Ahmed, M. Xiao, and Y. P. Zhang, RSC Adv. **5**, 39449 (2015).
35. R. W. Boyd, *Nonlinear Optics*, 3rd ed. (Academic, 2008).
36. J.-H. Wu, M. Artoni, and G. C. L. Rocca, J. Opt. Soc. Am. B **25**, 1840 (2008).
37. Y. Q. Zhang, X. Liu, M. R. Belić, Z. K. Wu, and Y. P. Zhang, Ann. Phys. **363**, 114 (2015).
38. I. Kaminer, R. Bekenstein, J. Nemirovsky, and M. Segev, Phys. Rev. Lett. **108**, 163901 (2012).
39. P. Zhang, Y. Hu, T. Li, D. Cannan, X. Yin, R. Morandotti, Z. Chen, and X. Zhang, Phys. Rev. Lett. **109**, 193901 (2012).
40. P. Aleahmad, M.-A. Miri, M. S. Mills, I. Kaminer, M. Segev, and D. N. Christodoulides, Phys. Rev. Lett. **109**, 203902 (2012).
41. P. Zhang, Y. Hu, D. Cannan, A. Salandrino, T. Li, R. Morandotti, X. Zhang, and Z. Chen, Opt. Lett. **37**, 2820 (2012).
42. Y. Lumer, Y. Liang, R. Schley, I. Kaminer, E. Greenfield, D. Song, X. Zhang, J. Xu, Z. Chen, and M. Segev, Optica **2**, 886 (2015).
43. Y. Q. Zhang, H. Zhong, M. R. Belić, C. B. Li, Z. Y. Zhang, F. Wen, Y. P. Zhang, and M. Xiao, Opt. Lett. **41**, 3273 (2016).
44. M. A. Bandres and B. M. Rodríguez-Lara, New J. Phys. **15**, 013054 (2013).
45. M. Abramowitz and I. A. Stegun, *Handbook of Mathematical Functions* (Dover, 1970).